Excitation Energies from Time-Dependent Density Functional Theory Using Exact and Approximate Potentials

M. Petersilka and E. K. U. Gross
Institut für Theoretische Physik, Universität Würzburg,
Am Hubland, 97074 Würzburg, Germany

Kieron Burke
Department of Chemistry, Rutgers University
610 Taylor Road, Piscataway, NJ 08854

July 26, 2000

Abstract

The role of the exchange-correlation potential and the exchange-correlation kernel in the calculation of excitation energies from time-dependent density functional theory is studied. Excitation energies of the helium and beryllium atoms are calculated, both from the exact Kohn-Sham ground-state potential, and from two orbital-dependent approximations. These are exact exchange and self-interaction corrected local density approximation (SIC-LDA), both calculated using Krieger-Li-Iafrate approximation. For the exchange-correlation kernels, three adiabatic approximations were tested: the local density approximation, exact exchange, and SIC-LDA. The choice of the ground-state exchange correlation potential has the largest impact on the absolute position of most excitation energies. In particular, orbital-dependent approximate potentials result in a uniform shift of the transition energies to the Rydberg states.

1 Introduction

The Hohenberg-Kohn theorem [1] of ground-state density functional theory (DFT) guarantees that every observable of a stationary physical system can be expressed in terms of its ground-state density. In principle, this is also true for the set of excited-state energies, and several extensions of ground-state DFT have been proposed [2]- [13]. Accurate calculations of excitation energies, however, remain a difficult subject. Recently, some of us proposed a different approach to the calculation of excitation energies [14], within the framework of time-dependent DFT (TDDFT) [15]. The central idea is to use the fact that the linear density response has poles at the physical excitation energies and can be calculated from the response function of a noninteracting Kohn-Sham (KS) system and a frequency-dependent Kohn-Sham (KS) kernel. In this way, we obtain the shifts of the KS orbital differences (which are the poles of the KS response function) towards the true excitation energies. Recent applications [16]- [25] suggest that this method may become a standard tool in quantum chemistry.

The success of any density functional method, however, depends on the quality of the functionals employed. In this article, we investigate the relative importance of the approximations inherent in the TDDFT formalism for the calculation of discrete excitation energies of finite systems. This mainly concerns the role of the ground-state XC potential, $v_{\rm xc}(\mathbf{r})$ compared to the dynamical XC kernel, $f_{\rm xc}(\mathbf{r},\mathbf{r}';\omega)$. For the helium and beryllium atoms, we compare the results obtained from using the exact XC potentials and two orbital dependent potentials, one based on the exact exchange expression and the other on the self-interaction corrected local density approximation [26], evaluated with the method of Krieger, Li and Iafrate (KLI) [27]- [31] in combination with three distinct approximations for the XC kernels, which are given in Sect. 2.2.

2 Formalism

2.1 Kohn-Sham equations for the frequency-dependent linear density response

The frequency dependent linear density response $n_{1\sigma}(\mathbf{r},\omega)$ of electrons with spin σ, reacting to a perturbation $v_{1\sigma'}$ of frequency ω can be written in terms of the interacting density-density response function $\chi_{\sigma\sigma'}$ by [32]

$$n_{1\,\sigma}(\mathbf{r},\omega) = \sum_{\sigma'} \int d^3r'\, \chi_{\sigma\sigma'}(\mathbf{r},\mathbf{r}';\omega)\, v_{1\,\sigma'}(\mathbf{r}',\omega)\,. \tag{1}$$

In the spin-dependent version [33] of time-dependent DFT [15], the density response $n_{1\sigma}$ can be expressed in terms of the response function $\chi_{s\,\sigma\sigma'}$ of the non-interacting Kohn-Sham (KS) system [14, 34]:

$$n_{1\,\sigma}(\mathbf{r},\omega) = \sum_{\sigma'} \int d^3r'\, \chi_{{\rm s}\,\sigma\sigma'}(\mathbf{r},\mathbf{r}';\omega)\, v_{{\rm s},1\,\sigma'}(\mathbf{r}',\omega)\,. \tag{2}$$

The KS response function

$$\chi_{{\rm s}\,\sigma\sigma'}(\mathbf{r},\mathbf{r}';\omega) = \delta_{\sigma\sigma'} \sum_{j,k} (f_{k\sigma} - f_{j\sigma}) \frac{\varphi_{j\sigma}(\mathbf{r})\varphi^*_{k\sigma}(\mathbf{r})\varphi^*_{j\sigma}(\mathbf{r}')\varphi_{k\sigma}(\mathbf{r}')}{\omega - (\epsilon_{j\sigma} - \epsilon_{k\sigma}) + i\eta} \tag{3}$$

is readily expressed in terms of the unperturbed static Kohn-Sham orbitals $\varphi_{k\sigma}$ (with occupation numbers $f_{j\sigma}$). Relation (2) contains the linearized KS potential

$$v_{{\rm s},1\,\sigma}(\mathbf{r},\omega) = v_{1\sigma}(\mathbf{r},\omega) + \sum_{\sigma'} \int d^3r'\, \frac{n_{1\sigma'}(\mathbf{r}',\omega)}{|\mathbf{r}-\mathbf{r}'|} + \sum_{\sigma'} \int d^3r'\, f_{{\rm xc}\,\sigma\sigma'}(\mathbf{r},\mathbf{r}';\omega)\, n_{1\sigma'}(\mathbf{r}',\omega)\,. \tag{4}$$

in which the spin-dependent exchange-correlation (XC) kernel $f_{\rm xc}$ is defined as the Fourier transform of

$$f_{{\rm xc}\,\sigma\sigma'}[n_{0\uparrow}, n_{0\downarrow}](\mathbf{r},t,\mathbf{r}',t') := \left.\frac{\delta v_{{\rm xc}\,\sigma}[n_\uparrow, n_\downarrow](\mathbf{r},t)}{\delta n_{\sigma'}(\mathbf{r}',t')}\right|_{n_{0\uparrow},n_{0\downarrow}}\,. \tag{5}$$

Given an approximation to $f_{\rm xc}$, Eqs. (2) and (4) can be solved self-consistently for every frequency ω.

2.2 Approximations for the exchange-correlation kernel

For spin-unpolarized ground states, there are only two independent combinations of the spin components of the XC kernel, since $f_{\mathrm{xc}\uparrow\uparrow} = f_{\mathrm{xc}\downarrow\downarrow}$ and $f_{\mathrm{xc}\uparrow\downarrow} = f_{\mathrm{xc}\downarrow\uparrow}$:

$$f_{\mathrm{xc}} = \frac{1}{4}\sum_{\sigma\sigma'} f_{\mathrm{xc}\,\sigma\sigma'} = \frac{1}{2}(f_{\mathrm{xc}\uparrow\uparrow} + f_{\mathrm{xc}\uparrow\downarrow}) \qquad G_{\mathrm{xc}} = \frac{1}{4}\sum_{\sigma\sigma'} \sigma\sigma' f_{\mathrm{xc}\,\sigma\sigma'} = \frac{1}{2}(f_{\mathrm{xc}\uparrow\uparrow} - f_{\mathrm{xc}\uparrow\downarrow}), \quad (6)$$

(contrary to common usage, we have not separated the Bohr magneton in the definition of G_{xc}). Note that $f_{\mathrm{x}} = G_{\mathrm{x}}$, as exchange contains only parallel spin contributions.

The simplest possible approximation is the adiabatic local (spin-)density approximation [35] (ALDA). For spin-unpolarized ground states, this leads to

$$f_{\mathrm{xc}}^{\mathrm{ALDA}}[n](\mathbf{r},\mathbf{r}') = \delta(\mathbf{r}-\mathbf{r}')\left.\frac{d^2 e_{\mathrm{xc}}^{\mathrm{hom}}}{d\rho^2}\right|_{\rho=n(\mathbf{r}),\zeta=0}, \qquad G_{\mathrm{xc}}^{\mathrm{ALDA}}[n](\mathbf{r},\mathbf{r}') = \delta(\mathbf{r}-\mathbf{r}')\frac{\alpha_{\mathrm{xc}}(n(\mathbf{r}))}{n(\mathbf{r})}, \quad (7)$$

where $e_{\mathrm{xc}}^{\mathrm{hom}}$ is the exchange-correlation energy per unit volume of the homogeneous electron gas, ζ is the relative spin polarization, $(n_\uparrow - n_\downarrow)/n$, and the spin-stiffness $\alpha_{\mathrm{xc}} = \frac{\delta^2}{\delta\zeta^2}\left(e_{\mathrm{xc}}^{\mathrm{hom}}(\rho,\zeta)/\rho\right)\Big|_{\zeta=0}$.

Approximate XC functionals derived from the homogeneous electron gas suffer from several shortcomings, such as spurious self-interaction contributions. These are very significant for calculations of orbital eigenvalues, as they affect the asymptotic decay of the ground-state potential. For example, the XC potential in the local density approximation decays exponentially, so rapidly that only one virtual state is bound. An alternative approach towards the construction of improved functionals is to use perturbation theory in the electron-electron coupling constant[36]. This leads to orbital-dependent functionals, which can be solved self-consistently using the optimized effective potential method (OEP) [37]-[39]. In the time-dependent case, this method takes as a starting point a given (approximate) expression for the quantum mechanical action integral as a functional of a set of orbitals[40]. Variation with respect to a local effective potential then leads to an integral equation for the exchange-correlation potential. Given an exchange-correlation potential of that kind, the corresponding exchange-correlation kernel can be constructed in the same spirit [14, 41]. The essential steps are formally identical to the OEP construction of the exchange-correlation potential for the ground-state[42].

In the time-dependent X-only approximation, A_{xc} is replaced by[1]

$$A_{\mathrm{x-only}} = -(1/2)\sum_{\sigma}\sum_{i,j}^{N_\sigma}\int_{-\infty}^{t_1} dt \int d^3r \int d^3r'\; \phi_{i\sigma}^*(\mathbf{r}'t)\phi_{j\sigma}(\mathbf{r}'t)\phi_{i\sigma}(\mathbf{r}t)\phi_{j\sigma}^*(\mathbf{r}t) \,/\, |\mathbf{r}-\mathbf{r}'|\,. \quad (8)$$

The orbital-dependent exchange kernel in the time-dependent KLI approximation is [14, 41]

$$f_{\mathrm{x-only}\,\sigma\sigma'}^{\mathrm{TDOEP}}(\mathbf{r},\mathbf{r}') = -\delta_{\sigma\sigma'}\frac{1}{|\mathbf{r}-\mathbf{r}'|}\frac{\left|\sum_k f_{k\sigma}\,\varphi_{k\sigma}(\mathbf{r})\varphi_{k\sigma}^*(\mathbf{r}')\right|^2}{n_\sigma(\mathbf{r})n_\sigma(\mathbf{r}')}\,. \quad (9)$$

[1] In general, a Keldysh contour integral in complex time is needed [40] to avoid causality difficulties[43], except when the action is local in the orbitals in time, as is the case with all approximations tested here.

In general, the exact x-only kernel carries a frequency-dependence. This is not accounted for in the present approximation (9). However, for one- and spin-unpolarized two-electron systems, Eqs. (9) is the *exact* solution of the respective integral equations in the limit of a time-dependent X-only theory. This yields

$$f_{\rm x} = G_{\rm x} = -\frac{2|\sum_k f_k \varphi_k(\mathbf{r})\varphi_k^*(\mathbf{r}')|^2}{n(\mathbf{r})|\mathbf{r}-\mathbf{r}'|n(\mathbf{r}')} \qquad = \left(-\frac{1}{2|\mathbf{r}-\mathbf{r}'|} \quad \text{for} \quad 2 \quad \text{elec}\right). \tag{10}$$

Inherent to any X-only theory, the resulting kernels are lacking off-diagonal elements in spin space. To improve upon the X-only treatment, we use the self-interaction corrected (SIC) LDA [26] for $A_{\rm xc}$:

$$A_{\rm xc}^{\rm SIC} = \int_{-\infty}^{t_1} dt \left(E_{\rm xc}^{\rm LDA}[n_\uparrow(t), n_\downarrow(t)] - \sum_{i\sigma} E_{\rm xc}^{\rm LDA}[n_{i\sigma}(t), 0] - \frac{1}{2}\sum_{i\sigma} \int d^3r \int d^3r' \frac{n_{i\sigma}(\mathbf{r},t)\, n_{i\sigma}(\mathbf{r}',t)}{|\mathbf{r}-\mathbf{r}'|} \right) \tag{11}$$

which is an orbital-dependent functional as well due to the explicit dependence on the orbital densities

$$n_{i\sigma}(\mathbf{r},t) = |\phi_{i\sigma}(\mathbf{r},t)|^2 \quad (i = 1, 2, \ldots, N/2)\,. \tag{12}$$

] An improvement over both ALDA and exact exchange might be provided by correcting ALDA for self-interaction error[26]. Within the adiabatic SIC-LDA, the exchange-correlation kernel reads

$$f_{{\rm xc}\,\sigma\sigma'}^{\rm TDOEP-SIC}(\mathbf{r},\mathbf{r}',\omega) = f_{{\rm xc}\,\sigma\sigma'}^{\rm ALDA}(\mathbf{r},\mathbf{r}',\omega) - \\ - \frac{\delta_{\sigma\sigma'}}{n_{0\,\sigma}(\mathbf{r})\, n_{0\,\sigma}(\mathbf{r}')} \sum_k f_{k\sigma} |\varphi_{k\sigma}(\mathbf{r})|^2 \, |\varphi_{k\sigma}(\mathbf{r}')|^2 \left(\frac{\delta v_{{\rm xc}\,\sigma}^{\rm LDA}(n_{k\,\sigma}(\mathbf{r}),0)}{\delta n_{k\,\sigma}(\mathbf{r}')} + \frac{1}{|\mathbf{r}-\mathbf{r}'|} \right). \tag{13}$$

This expression reduces to the exact result (Eq. (9)) for one electron. For more than one electron, spurious self-interaction parallel-spin contributions in ALDA are corrected, for both exchange and correlation. The correction has no affect on anti-parallel spin contributions, leaving simply the ALDA result. We find simply

$$f_{\rm xc}^{\rm SIC} = f_{\rm xc}^{\rm ALDA} + \Delta f_{\rm xc}^{\rm SIC} \qquad G_{\rm xc}^{\rm SIC} = G_{\rm xc}^{\rm ALDA} + \Delta f_{\rm xc}^{\rm SIC} \tag{14}$$

where

$$\Delta f_{\rm xc}^{\rm SIC} = -\frac{2\sum_k f_k n_k(\mathbf{r}) n_k(\mathbf{r}')}{n(\mathbf{r}) n(\mathbf{r}')} \left\{ \delta(\mathbf{r}-\mathbf{r}') \, \frac{\partial v_{{\rm xc},\uparrow}^{\rm hom}(n_k,0)}{\partial n_k(\mathbf{r})} + \frac{1}{|\mathbf{r}-\mathbf{r}'|} \right\}. \tag{15}$$

3 Calculation of excitation energies

The linear density response has poles at the exact excitation energies of the interacting system (see, e.g., [32]). The key idea is to start from a particular KS orbital energy difference $\epsilon_{j\sigma} - \epsilon_{k\sigma}$ (at which the Kohn-Sham response function (3) has a pole) and to use the formally exact representation (2) of the linear density response to calculate the shifts of the Kohn-Sham excitation energies towards the true excitation energies Ω. To extract

these shifts from the density response, we cast Eq. (2) together with (4) into the form of an integral equation for $n_{1\sigma}$:

$$\sum_{\nu'} \int d^3y' \quad \left[\delta_{\sigma\nu'} \delta(\mathbf{r}-\mathbf{y}') - \sum_{\nu} \int d^3y \chi_{\mathrm{s}\,\sigma\nu}(\mathbf{r},\mathbf{y};\omega) \left(\frac{1}{|\mathbf{y}-\mathbf{y}'|} + f_{\mathrm{xc}\,\nu\nu'}(\mathbf{y},\mathbf{y}';\omega) \right) \right] n_{1\nu'}(\mathbf{y}',\omega)$$
$$= \sum_{\nu} \int d^3y \, \chi_{\mathrm{s}\,\sigma\nu}(\mathbf{r},\mathbf{y};\omega) v_{1\nu}(\mathbf{y},\omega) \,. \tag{16}$$

In general, the true excitation energies Ω are not identical with the Kohn-Sham excitation energies $\epsilon_{j\sigma} - \epsilon_{k\sigma}$, and the right-hand side of Eq. (16) remains finite for $\omega \to \Omega$. The exact spin-density response $n_{1\sigma}$, on the other hand, exhibits poles at the true excitation energies Ω. Hence, the integral operator acting on $n_{1\sigma}$ on the left-hand side of Eq. (16) cannot be invertible for $\omega \to \Omega$. This means that the integral operator acting on the spin-density vector in Eq. (16) is non-invertible (i.e., has vanishing eigenvalues) at the physical excitation energies. Rigorously, the true excitation energies Ω are those frequencies where the eigenvalues $\lambda(\omega)$ of

$$\sum_{\nu'} \int d^3y' \sum_{\nu} \int d^3y \quad \chi_{\mathrm{s}\,\sigma\nu}(\mathbf{r},\mathbf{y};\omega) \left(\frac{1}{|\mathbf{y}-\mathbf{y}'|} + f_{\mathrm{xc}\,\nu\nu'}(\mathbf{y},\mathbf{y}';\omega) \right) \gamma_{\nu'}(\mathbf{y}',\omega) =$$
$$= \lambda(\omega) \gamma_{\sigma}(\mathbf{r},\omega) \tag{17}$$

satisfy

$$\lambda(\Omega) = 1 \,. \tag{18}$$

For notational brevity, we use double indices $q \equiv (j,k)$ to characterize an excitation energy; $\omega_{q\sigma} \equiv \epsilon_{j\sigma} - \epsilon_{k\sigma}$ denotes the excitation energy of the single-particle transition $(k\sigma \to j\sigma)$. Consequently, we set $\alpha_{q\sigma} := f_{k\sigma} - f_{j\sigma}$ and

$$\Phi_{q\sigma}(\mathbf{r}) := \varphi^*_{k\sigma}(\mathbf{r}) \varphi_{j\sigma}(\mathbf{r}) \tag{19}$$

as well as

$$\xi_{q\sigma}(\omega) := \sum_{\nu'} \int d^3y' \int d^3y \, \Phi_{q\sigma}(\mathbf{y})^* \left(\frac{1}{|\mathbf{y}-\mathbf{y}'|} + f_{\mathrm{xc}\,\sigma\nu'}(\mathbf{y},\mathbf{y}';\omega) \right) \gamma_{\nu'}(\mathbf{y}',\omega) \,. \tag{20}$$

Without any approximation, equation (17) can be cast [16] into matrix form

$$\sum_{\sigma'} \sum_{q'} \frac{M_{q\sigma\,q'\sigma'}(\omega)}{\omega - \omega_{q'\sigma'} + i\eta} \xi_{q'\sigma'}(\omega) = \lambda(\omega) \xi_{q\sigma}(\omega) \,, \tag{21}$$

with the matrix elements

$$M_{q\sigma\,q'\sigma'}(\omega) = \alpha_{q'\sigma'} \int d^3r \int d^3r' \, \Phi^*_{q\sigma}(\mathbf{r}) \left(\frac{1}{|\mathbf{r}-\mathbf{r}'|} + f_{\mathrm{xc}\,\sigma\sigma'}(\mathbf{r},\mathbf{r}';\omega) \right) \Phi_{q'\sigma'}(\mathbf{r}') \,. \tag{22}$$

At the frequencies $\omega = \Omega$, Eq. (21) can be written as

$$\sum_{q'\sigma'} \left(M_{q\sigma\,q'\sigma'}(\Omega) + \delta_{q\sigma\,q'\sigma'} \omega_{q\sigma} \right) \beta_{q'\sigma'}(\Omega) = \Omega \beta_{q\sigma}(\Omega) \,, \tag{23}$$

where we have defined

$$\beta_{q\sigma}(\Omega) := \xi_{q\sigma}(\Omega)/(\Omega - \omega_{q\sigma})\,. \tag{24}$$

The solutions Ω of the nonlinear matrix-equation (23) are the physical excitation energies. The inevitable truncation of the infinite-dimensional matrix in Eq. (23) amounts to the approximation of $\chi^{(0)}$ by a finite sum

$$\chi^{(0)}(\mathbf{r},\mathbf{r}',\omega) \approx \sum_{\sigma=\uparrow\downarrow}\sum_{q}^{Q} \alpha_q \frac{\Phi_q(\mathbf{r})\Phi_q(\mathbf{r}')}{\omega - \omega_{q\sigma}}\,. \tag{25}$$

This truncation explicitly takes into account numerous poles of the noninteracting response function. In any adiabatic approximation to the XC kernel, the matrix elements $M_{q\sigma\, q'\sigma'}$ are real and frequency independent. In this case the excitation energies Ω are simply the eigenvalues of the $(Q \times Q)$ matrix $M_{q\sigma\, q'\sigma'}(\Omega = 0) + \delta_{q\sigma,q'\sigma'}\omega_{q\sigma}$. For bound states of finite systems we encounter well-separated poles in the linear density response. In our calculations, we include many such poles, but only those of bound states, ignoring continuum contributions. The nature and size of the error this introduces has been studied by van Gisbergen et al.[21], and does not affect the qualitative conclusions found in this work.

A simple and extremely instructive case is when we expand about a single KS-orbital energy difference $\omega_{p\tau}$ [14, 16]. The physical excitation energies Ω are then given by the solution of

$$\lambda(\Omega) = \frac{A(\omega_{p\tau})}{\Omega - \omega_{p\tau}} + B(\omega_{p\tau}) + \ldots = 1\,. \tag{26}$$

For non-degenerate single-particle poles $\omega_{p\tau}$, the coefficients in Eq. (26) are given by

$$A(\omega_{p\tau}) = M_{p\tau\, p\tau}(\omega_{p\tau}) \tag{27}$$

and

$$B(\omega_{p\tau}) = \left.\frac{dM_{p\tau p\tau}}{d\omega}\right|_{\omega_{p\tau}} + \frac{1}{M_{p\tau p\tau}(\omega_{p\tau})} \sum_{q'\sigma' \neq p\tau} \frac{M_{p\tau\, q'\sigma'}(\omega_{p\tau}) M_{q'\sigma'\, p\tau}(\omega_{p\tau})}{\omega_{p\tau} - \omega_{q'\sigma'} + i\eta}\,. \tag{28}$$

If the pole $\omega_{p\tau}$ is $\wp$-fold degenerate, $\omega_{p_1\tau_1} = \omega_{p_2\tau_2} = \ldots = \omega_{p_\wp\tau_\wp} \equiv \omega_0$, the lowest-order coefficient A in Eq. (26) is determined by a $\wp$-dimensional matrix equation

$$\sum_{k=1}^{\wp} M_{p_i\tau_i\, p_k\tau_k}(\omega_0)\xi^{(n)}_{p_k\tau_k} = A_n(\omega_0)\xi^{(n)}_{p_i\tau_i}\,, \quad i = 1\ldots\wp\,, \tag{29}$$

with $\wp$ different solutions $A_1 \ldots A_\wp$. For excitation energies Ω close to ω_0, the lowest-order term of the above Laurent expansion will dominate the series. In this single-pole approximation (SPA), the excitation energies Ω satisfy Eq. (26) reduces to

$$\lambda_n(\Omega) \approx \frac{A_n(\omega_0)}{\Omega - \omega_0} = 1\,. \tag{30}$$

The condition (18) and its complex conjugate, $\lambda^*(\Omega) = 1$, finally lead to a compact expression for the excitation energies.

$$\Omega_n \approx \omega_0 + \Re A_n(\omega_0)\,. \tag{31}$$

For closed-shell systems, every Kohn-Sham orbital eigenvalue is degenerate with respect to spin, i.e. the spin multiplet structure is absent in the bare Kohn-Sham eigenvalue spectrum. Within the SPA, the dominant terms in the corrections to the Kohn-Sham eigenvalues towards the true multiplet energies naturally emerge from the solution of the (2×2) eigenvalue problem

$$\sum_{\sigma'=\uparrow,\downarrow} M_{p\sigma p\sigma'}(\omega_0)\xi_{p\sigma'}(\omega_0) = A\xi_{p\sigma}(\omega_0)\,. \tag{32}$$

Then, the resulting excitation energies are:

$$\Omega_{1,2} = \omega_0 + \Re\left\{M_{p\uparrow p\uparrow} \pm M_{p\uparrow p\downarrow}\right\}\,. \tag{33}$$

Using the explicit form of the matrix elements (22) one finds[2]

$$\Omega_1 = \omega_0 + 2\Re \int d^3r \int d^3r'\, \Phi_p^*(\mathbf{r}) \left(\frac{1}{|\mathbf{r}-\mathbf{r}'|} + f_{\rm xc}(\mathbf{r},\mathbf{r}';\omega_0)\right) \Phi_p(\mathbf{r}') \tag{34}$$

$$\Omega_2 = \omega_0 + 2\Re \int d^3r \int d^3r'\, \Phi_p^*(\mathbf{r}) G_{\rm xc}(\mathbf{r},\mathbf{r}';\omega_0) \Phi_p(\mathbf{r}')\,. \tag{35}$$

The kernel $G_{\rm xc}$ embraces the exchange and correlation effects in the Kohn-Sham equation for the linear response of the frequency-dependent magnetization density $m(\mathbf{r},\omega)$ [33]. For unpolarized systems, the weight of the pole in the spin-summed susceptibility (both for the Kohn-Sham and the physical systems) at Ω_2 is exactly zero, indicating that these are the optically forbidden transitions to triplet states. The singlet excitation energies are at Ω_1. In this way, the SPA already gives rise to a spin-multiplet structure in the excitation spectrum. We use SPA to understand the results of different approximations, since it simply relates the calculated shifts from KS eigenvalues to matrix elements of the XC kernel.

At this point we stress that the TDDFT formalism for the calculation of excitation energies involves three different types of approximations:

1. In the calculation of the Kohn-Sham orbitals $\varphi_k(\mathbf{r})$ and their eigenvalues ϵ_k, one employs some approximation of the static XC potential $v_{\rm xc}$.

2. Given the stationary Kohn-Sham orbitals and the ground state density, the functional form of the XC kernel $f_{{\rm xc}\,\sigma\sigma'}$ needs to be approximated in order to calculate the matrix elements defined in Eq. (22).

3. Once the matrix elements are obtained, the infinite-dimensional eigenvalue problem (21) (or, equivalently, (23)) must be truncated in one way or another.

In the following, we are going to investigate the relative importance of the approximations (1.) and (2.). Furthermore, truncation effects will be estimated by comparing the results obtained in SPA (34,35) with the solution of the "full" problem (23) which is based on using up to 38 bound virtual orbitals.

[2]Since we are dealing with spin saturated systems, we have dropped the spin-index of $\Phi_{p\sigma}$.

Table 1: Singlet excitation energies of neutral helium, calculated from the exact XC potential by using approximate XC kernels (in atomic units)

		ALDA (xc)		TDOEP (x-only)		TDOEP (SIC)		
$k \to j$	ω_{jk}	SPA	full[a]a	SPA	full[a]	SPA	full[a]	exact[b]
$1s \to 2s$	0.7460	0.7718	0.7678	0.7687	0.7659	0.7674	0.7649	0.7578
$1s \to 3s$	0.8392	0.8458	0.8461	0.8448	0.8450	0.8445	0.8448	0.8425
$1s \to 4s$	0.8688	0.8714	0.8719	0.8710	0.8713	0.8709	0.8712	0.8701
$1s \to 5s$	0.8819	0.8832	0.8835	0.8830	0.8832	0.8829	0.8832	0.8825
$1s \to 6s$	0.8888	0.8895	0.8898	0.8894	0.8896	0.8894	0.8895	0.8892
$1s \to 2p$	0.7772	0.7764	0.7764	0.7850	0.7844	0.7836	0.7833	0.7799
$1s \to 3p$	0.8476	0.8483	0.8483	0.8500	0.8501	0.8497	0.8498	0.8486
$1s \to 4p$	0.8722	0.8726	0.8726	0.8732	0.8733	0.8731	0.8732	0.8727
$1s \to 5p$	0.8836	0.8838	0.8838	0.8841	0.8842	0.8841	0.8841	0.8838
$1s \to 6p$	0.8898	0.8899	0.8899	0.8901	0.8901	0.8900	0.8901	0.8899
Mean abs. dev.[c]	0.0022	0.0023	0.0021	0.0022	0.0020	0.0019	0.0017	
Mean rel. dev.[d]	0.28%	0.30%	0.26%	0.28%	0.25%	0.24%	0.21%	

[a]Using the lowest 34 unoccupied orbitals of s and p symmetry, respectively.
[b]Nonrelativistic variational calculation [38].
[c]Mean value of the absolute deviations from the exact values.

4 Results for the Helium Atom

In this section we report numerical results for excitation energies of the He atom. The stationary Kohn-Sham equations were solved numerically on a radial grid (i.e. without basis set expansion) using a large number of semi-logarithmically distributed grid points [44] up to a maximum radius of several hundred atomic units in order to achieve high accuracy the Rydberg states ($n \geq 10$) as well.

4.1 Exact Kohn-Sham potential

To eliminate the errors (1.) associated with the approximation for the ground-state KS potential, we employ the *exact* XC potential of the He atom to generate the stationary Kohn-Sham orbitals $\varphi_k(\mathbf{r})$ and their eigenvalues ϵ_k. This isolates the effects which exclusively arise due to the approximations (2.) and (3.). The potential data provided by Umrigar and Gonze [45] were interpolated nonlinearly for $r \leq 10$ atomic units. Around $r = 10$ atomic units, the XC potential is almost identical to $-1/r$. This behavior was used as an extrapolation of the exact exchange-correlation potential to larger distances.

Tables 1 and 2 show the excitation energies of neutral helium calculated with the exact exchange-correlation potential. The results are compared with a highly accurate nonrelativistic variational calculation [46] of the eigenstates of Helium. It is a remarkable fact that the Kohn-Sham excitation energies $\omega_{jk} = \epsilon_j - \epsilon_k$ are already very close to the exact spectrum, and, at the same time, are always in between the singlet and the triplet energies[47, 48].

Based on these eigenvalue differences, we have calculated the shifts towards the true excitation energies using several approximations for the exchange-correlation kernels f_{xc}:

Table 2: Triplet excitation energies of neutral helium, calculated from the exact XC potential by using approximate XC kernels (in atomic units)

		ALDA (xc)		TDOEP (x-only)		TDOEP (SIC)		
$k \to j$	ω_{jk}	SPA	full[a]	SPA	full[a]	SPA	full[a]	exact[b]
$1s \to 2s$	0.7460	0.7357	0.7351	0.7232	0.7207	0.7313	0.7300	0.7285
$1s \to 3s$	0.8392	0.8366	0.8368	0.8337	0.8343	0.8353	0.8356	0.8350
$1s \to 4s$	0.8688	0.8678	0.8679	0.8667	0.8671	0.8673	0.8675	0.8672
$1s \to 5s$	0.8819	0.8814	0.8815	0.8808	0.8811	0.8811	0.8813	0.8811
$1s \to 6s$	0.8888	0.8885	0.8885	0.8882	0.8883	0.8884	0.8884	0.8883
$1s \to 2p$	0.7772	0.7702	0.7698	0.7693	0.7688	0.7774	0.7774	0.7706
$1s \to 3p$	0.8476	0.8456	0.8457	0.8453	0.8453	0.8471	0.8471	0.8456
$1s \to 4p$	0.8722	0.8714	0.8715	0.8712	0.8713	0.8720	0.8720	0.8714
$1s \to 5p$	0.8836	0.8832	0.8832	0.8831	0.8831	0.8834	0.8835	0.8832
$1s \to 6p$	0.8898	0.8895	0.8895	0.8895	0.8895	0.8897	0.8897	0.8895
Mean abs. dev.[c]	0.0035	0.0010	0.0011	0.0009	0.0011	0.0013	0.0012	
Mean rel. dev.	0.45%	0.14%	0.14%	0.12%	0.15%	0.16%	0.15%	

[a]Using the lowest 34 unoccupied orbitals of s and p symmetry, respectively.
[b]Nonrelativistic variational calculation [38].
[c]Mean value of the absolute deviations from the exact values.

- The adiabatic local density approximation (ALDA), with the inclusion of correlation contributions in the parametrization of Vosko, Wilk and Nusair [49].
- The approximate X-only time-dependent OEP (TDOEP) kernel of Eq. (9), which is based on the time-dependent Fock expression, and
- The approximate TDOEP-SIC kernel from Eq. (13) with the parametrization of Ref. [49] for the correlation contributions.

The columns denoted by "full" show the corresponding excitation energies Ω_i which are obtained as eigenvalues obtained from the (truncated) matrix equation (23). To investigate the effects of the truncation of the matrix equation (23) we compare the difference between the single-pole approximation (SPA) and the fully coupled results. The matrix equation (23) was solved using $N = 34$ unoccupied Kohn-Sham orbitals of s or p symmetry. For each symmetry class the resulting dimension of the (fully coupled but truncated) matrix in Eq. (23) is $(4N \times 4N)$ (due to the spin-degeneracy of the KS orbitals of Helium and the fact that the frequency-dependent Kohn-Sham response function is symmetric in the complex plane with respect to the imaginary axis). Thereby, convergence of the results to within 10^{-6} atomic units was reached within the space of bound states. When comparing the results from the SPA with the results from the fully coupled matrix, we observe only a small change in the resulting excitation energies (from a few hundredth of a percent to at most one half percent), independent of the functional form of the exchange-correlation kernel. Thus we conclude that in helium the single-pole approximation gives the dominant correction to the Kohn-Sham excitation spectrum. Hence, starting from the Kohn-Sham eigenvalue differences as zeroth order approximation to the excitation energies, the SPA can be used for the assignment of the excitation energies which are obtained as eigenvalues from

Eq. (23). Recent studies using basis set expansions [21] indicate that further improvement of the fully coupled results can be expected from the inclusion of continuum states. The general trends of the results however, are not affected.

In figure 1 we have plotted some typical excitation energies taken from the column headed "full" of table 1 and 2, We can understand the trends in this figure by analyzing

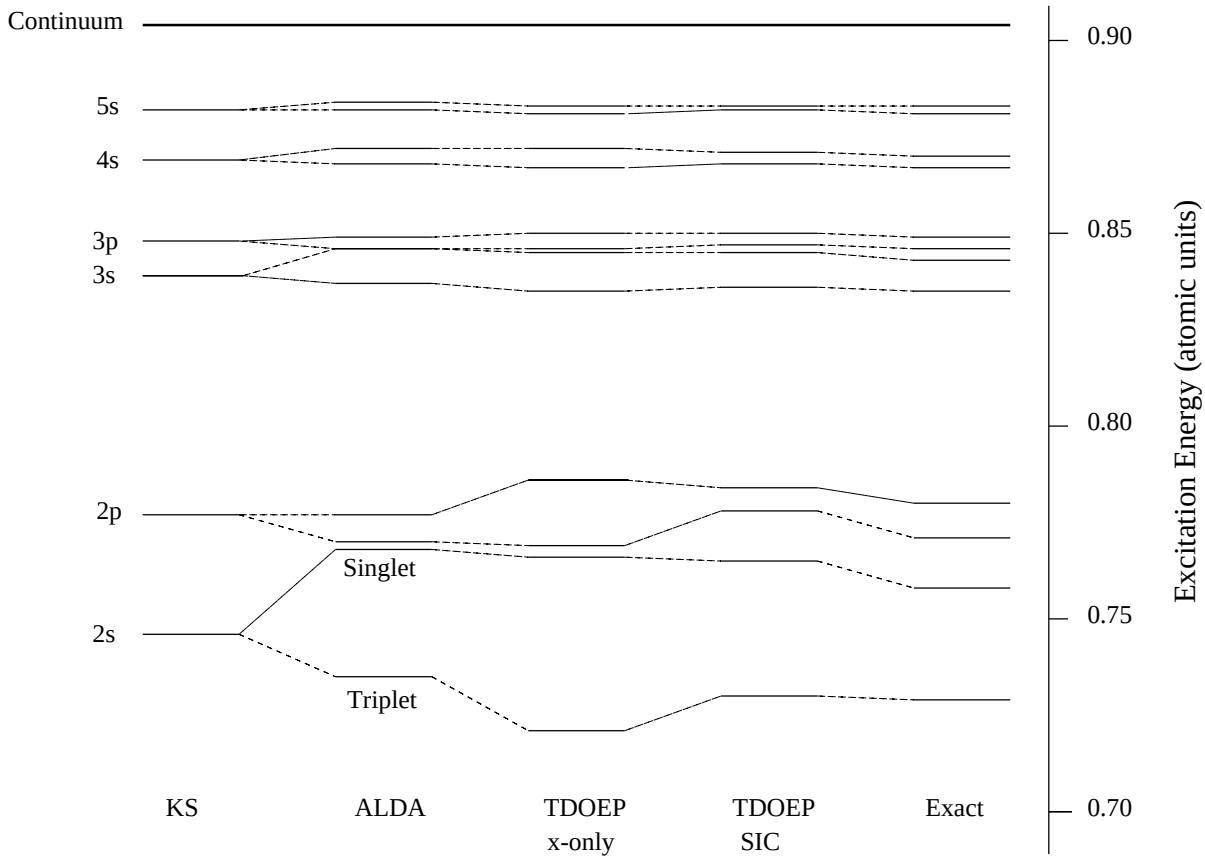

Figure 1: Typical excitation energies of He, including the orbital eigenvalues of the exact Kohn-Sham potential (KS) and the corrections from time-dependent density functional theory calculated within the adiabatic local density approximation (ALDA), with orbital dependent functionals in the X-only limit (TDOEP X-only) and the self-interaction corrected version of the ALDA (TDOEP-SIC).

the results in terms of the single-pole approximation. For the single-particle excitations in helium, the single-pole approximation leads to two-dimensional matrix equations for the excitation energies (c.f. Eqs. (32) - (34)). In the following, the notation

$$\langle \hat{\mathcal{O}} \rangle := \int d^3r \int d^3r' \, \Phi_p^*(\mathbf{r}) \hat{\mathcal{O}}(\mathbf{r}, \mathbf{r}') \Phi_p(\mathbf{r}') \tag{36}$$

will be used for the matrix elements of the two particle operators $\hat{\mathcal{O}}$ involved in the calcu-

Table 3: Singlet-triplet separations in helium obtained from Eq. (23), using the lowest 34 unoccupied orbitals of s and p symmetry of the exact XC potential and employing various approximate XC kernels. All values are in mHartrees.

	ALDA		TDOEP		
State	X-only	xc[a]	X-only	SIC	exact[b]
$2S$	42.2	32.7	45.2	34.9	29.3
$3S$	11.1	9.4	10.8	9.2	7.4
$4S$	4.7	4.0	4.3	3.7	2.9
$5S$	2.4	2.1	2.2	1.9	1.4
$6S$	1.4	1.3	1.2	1.1	0.8
$2P$	16.7	6.6	15.6	5.8	9.3
$3P$	4.5	2.6	4.7	2.7	2.9
$4P$	1.8	1.1	2.0	1.2	1.3
$5P$	0.9	0.6	1.0	0.7	0.6
$6P$	0.5	0.3	0.6	0.4	0.4
dev.[c]	3.0	1.1	3.1	1.3	
rel. dev.	55%	27%	56%	21%	

[a]Including correlation contributions in the form of Vosko, Wilk and Nusair [49].
[b]Taken from Ref. [46]
[c]Mean absolute deviation from the exact values

lation. Then, in the SPA,

$$\Omega_p^{\rm singlet} = \omega_p + 2\langle W\rangle + 2\langle f_{\rm xc}\rangle,\ \Omega_p^{\rm triplet} = \omega_p + 2\langle G_{\rm xc}\rangle,\ \Delta\Omega_p = 2(\langle W\rangle + \langle f_{\rm c}\rangle - \langle G_{\rm c}\rangle), \quad (37)$$

where $\Delta\Omega_p$ is the singlet-triplet splitting. Within the various approximations to the kernel, these levels become

$$\begin{aligned}
\Omega_p^{\rm sing} &= \omega_p + \langle W\rangle, & \Omega_p^{\rm triplet} &= \omega_p - \langle W\rangle, & ({\rm X-only}) \quad (38)\\
&= \omega_p + 2\langle W\rangle + 2\langle f_{\rm xc}^{\rm ALDA}\rangle, & &= \omega_p + 2\langle G_{\rm xc}^{\rm ALDA}\rangle, & {\rm ALDA} \quad (39)\\
&= \omega_p + \langle W\rangle + 2\langle f_{\rm c}^{\rm ALDA}\rangle - \langle f_{\rm c}^{\rm orb}\rangle, & &= \omega_p - \langle W\rangle + 2\langle G_{\rm c}^{\rm ALDA}\rangle - \langle f_{\rm c}^{\rm orb}\rangle. & {\rm SIC} \quad (40)
\end{aligned}$$

We begin our analysis with the splitting. In the simplest case, the TDOEP X-only kernel, we see that the singlet transitions are always overestimated, while the triplets are always underestimated. Since our TDOEP treatment is exact for exchange in this case, this underscores the importance of correlation. In particular, since $\langle f_{\rm x}\rangle = \langle G_{\rm x}\rangle = -\langle W\rangle/2$, the splitting is just $2\langle W\rangle$. This matrix element is always positive, correctly putting the singlet above the triplet, but the splitting is typically far too big. We demonstrate the effect of this in table 3, in which we compare splittings with and without correlation. To see why inclusion of correlation always reduces the splitting, we note the sign and magnitude of matrix elements, within ALDA. Even though both $\langle f_{\rm xc}^{\rm ALDA}\rangle$ and $\langle G_{\rm xc}^{\rm ALDA}\rangle$ are negative, because they are dominated by their exchange contributions, we find

$$\langle f_{\rm c}^{\rm ALDA}\rangle < -\langle G_{\rm c}^{\rm ALDA}\rangle < 0 \quad (41)$$

because in Eq. (6) antiparallel correlation dominates over parallel correlation. Thus the ALDA correlation contribution to the splitting is always negative in SPA. Note that the SIC

treatment of the splitting is only marginally better than in ALDA because, within SPA, the SIC splitting is identical to that of ALDA.

To analyze the separate levels, we need the magnitude of the SIC corrections:

$$\langle f_{\rm c}^{\rm ALDA}\rangle < \langle f_{\rm c}^{\rm orb}\rangle := \langle \frac{\delta v_{\rm c}^{\rm LDA}[n_{k\sigma},0]}{\delta n_{k\sigma}}\rangle < 0\,, \tag{42}$$

but the numerical values of both matrix elements differ by less than 8%. Moreover,

$$\langle G_{\rm c}^{\rm ALDA}\rangle > |\langle f_{\rm c}^{\rm orb}\rangle| > 0\,. \tag{43}$$

Looking at the *singlet* excitation energies of table 1 we see that in ALDA, the s-levels are too high (up to 10 mH), whereas the p-levels are too low (by up to 0.4 mH). In X-only TDOEP, the s-levels drop (by up to 3 mH), approaching the exact values, but the rise of the p-states (by up to 8mH) is too high. Incorporating explicit correlation terms by using the TDOEP-SIC kernel, the singlet lines correctly drop further (in comparison to the X-only results by up to 1 mH) since $2\langle f_{\rm c}^{\rm ALDA}\rangle - \langle f_{\rm c}^{\rm orb}\rangle \approx \langle f_{\rm c}^{\rm ALDA}\rangle$ in Eq. (40) is always a negative contribution. But still, the p-states are too high. Regarding the *triplet* excitation energies of table 2, the ALDA s-states are too high by at most 6mH, but the p-states are almost identical to the exact values. In X-only TDOEP, the triplet states experience a strong downshift from the Kohn-Sham excitation energies up to 25 mH, originating from the term $-\langle W\rangle$ (see Eq. (40)). In TDOEP-SIC, this downshift is partly screened by the positive correlation contributions $2\langle G_{\rm c}^{\rm ALDA}\rangle - \langle f_{\rm c}^{\rm orb}\rangle$, as can be seen from Eqs. (40), (42) and (43). This leads to an excellent agreement with the exact values for the s-states. However, these correlation terms are too large for the p-states. Since $\langle G_{\rm c}^{\rm ALDA}\rangle > \langle f_{\rm c}^{\rm ALDA}\rangle$, the rise of the triplet is always bigger than the dropping of the singlet.

4.2 Approximate Kohn-Sham potentials

Next we explore the effect of approximate exchange-correlation potentials $v_{\rm xc}$ on the calculated excitation spectrum of the He atom. We do not even report results within LDA and generalized gradient approximations (GGA)[50], since these potentials only support a few virtual states, so that many of the transitions reported here do not even exist in such calculations. (This problem is worst in small atoms, is less pronounced in molecules, and irrelevant in solids).

To produce a correct Rydberg series, the XC potential must decay as $-1/r$, an exact exchange effect. Hence we examine the OEP X-only potential (which, *for two-electron systems* is identical to the Hartree-Fock potential) and the OEP-SIC [31] potential. Both potentials show the correct behavior for large distances from the nucleus, and support of all the Rydberg states is guaranteed.

Tables 4 and 5 show the approximate Kohn-Sham excitation energies and the corresponding corrected excitation energies calculated from the approximate Kohn-Sham eigenvalues and orbitals of the X-only potential; tables 6 and 7 are their analogs from the OEP-SIC calculation. The Kohn-Sham orbital energy differences are almost uniformly shifted to larger values compared to the orbital energy differences of the exact Kohn-Sham potential. The shift ranges from 13.6 mH for the lowest excitation energy to 14.2 mH for excitation energies Ω_n with $n \geq 4$ for the X-only potential. The latter shift is exactly the difference

Table 4: Singlet excitation energies of neutral helium, calculated from the X-only potential and by using approximate XC kernels (in atomic units).

		ALDA (xc)		TDOEP (X-only)		
Transition	ω_{jk}	SPA	full[a]	SPA	full[a]	exact[b]
$1s \to 2s$	0.7596	0.7852	0.7812	0.7822	0.7794	0.7578
$1s \to 3s$	0.8533	0.8598	0.8601	0.8588	0.8591	0.8425
$1s \to 4s$	0.8830	0.8856	0.8860	0.8851	0.8855	0.8701
$1s \to 5s$	0.8961	0.8973	0.8977	0.8971	0.8974	0.8825
$1s \to 6s$	0.9030	0.9037	0.9040	0.9036	0.9038	0.8892
$1s \to 2p$	0.7905	0.7900	0.7900	0.7986	0.7981	0.7799
$1s \to 3p$	0.8616	0.8623	0.8623	0.8640	0.8641	0.8486
$1s \to 4p$	0.8864	0.8867	0.8867	0.8874	0.8875	0.8727
$1s \to 5p$	0.8978	0.8980	0.8980	0.8983	0.8984	0.8838
$1s \to 6p$	0.9040	0.9041	0.9041	0.9043	0.9043	0.8899
Mean abs. dev.[c]	0.0118	0.0156	0.0153	0.0162	0.0161	
Mean percentage error	1.37%	1.85%	1.81%	1.93%	1.90%	

[a]Using the lowest 34 unoccupied orbitals of s and p symmetry, respectively.
[b]Nonrelativistic variational calculation [38].
[c]Mean value of the absolute deviations from the exact values.

Table 5: Triplet excitation energies of neutral helium, calculated from the X-only potential and by using approximate XC kernels (in atomic units).

		ALDA (xc)		TDOEP (X-only)		
Transition	ω_{jk}	SPA	full[a]	SPA	full[a]	exact[b]
$1s \to 2s$	0.7596	0.7493	0.7488	0.7370	0.7345	0.7285
$1s \to 3s$	0.8533	0.8507	0.8508	0.8478	0.8484	0.8350
$1s \to 4s$	0.8830	0.8820	0.8821	0.8809	0.8812	0.8672
$1s \to 5s$	0.8961	0.8956	0.8957	0.8950	0.8953	0.8811
$1s \to 6s$	0.9030	0.9027	0.9028	0.9024	0.9026	0.8883
$1s \to 2p$	0.7905	0.7833	0.7830	0.7824	0.7819	0.7706
$1s \to 3p$	0.8616	0.8595	0.8596	0.8591	0.8592	0.8456
$1s \to 4p$	0.8864	0.8855	0.8856	0.8853	0.8854	0.8714
$1s \to 5p$	0.8978	0.8973	0.8974	0.8972	0.8973	0.8832
$1s \to 6p$	0.9040	0.9037	0.9037	0.9037	0.9037	0.8895
Mean abs. dev.[c]	0.0175	0.0149	0.0149	0.0130	0.0129	
Mean percentage error	2.11%	1.78%	1.78%	1.53%	1.51%	

[a]Using the lowest 34 unoccupied orbitals of s and p symmetry, respectively.
[b]Nonrelativistic variational calculation [38].
[c]Mean value of the absolute deviations from the exact values.

Table 6: Singlet excitation energies of neutral helium, calculated from the SIC-LDA potential and by using approximate XC kernels (in atomic units).

		ALDA (xc)		TDOEP (SIC)		
Transition	ω_{jk}	SPA	full[a]	SPA	full[a]	exact[b]
$1s \to 2s$	0.7838	0.8111	0.8070	0.8065	0.8039	0.7578
$1s \to 3s$	0.8825	0.8891	0.8895	0.8878	0.8881	0.8425
$1s \to 4s$	0.9130	0.9156	0.9161	0.9150	0.9154	0.8701
$1s \to 5s$	0.9263	0.9276	0.9280	0.9273	0.9276	0.8825
$1s \to 6s$	0.9333	0.9340	0.9343	0.9339	0.9341	0.8892
$1s \to 2p$	0.8144	0.8145	0.8144	0.8222	0.8217	0.7799
$1s \to 3p$	0.8906	0.8915	0.8915	0.8929	0.8930	0.8486
$1s \to 4p$	0.9163	0.9167	0.9167	0.9172	0.9173	0.8727
$1s \to 5p$	0.9280	0.9282	0.9282	0.9285	0.9285	0.8838
$1s \to 6p$	0.9343	0.9344	0.9344	0.9346	0.9346	0.8899
Mean abs. dev.[c]	0.0406	0.0446	0.0443	0.0449	0.0447	
Mean percentage error	4.74%	5.25%	5.21%	5.29%	5.26%	

[a]Using the lowest 34 unoccupied orbitals of s and p symmetry, respectively.
[b]Nonrelativistic variational calculation [38].
[c]Mean value of the absolute deviations from the exact values.

Table 7: Triplet excitation energies of neutral helium, calculated from the SIC-LDA potential and by using approximate XC kernels (in atomic units).

		ALDA (xc)		TDOEP (SIC)		
Transition	ω_{jk}	SPA	full[a]	SPA	full[a]	exact[b]
$1s \to 2s$	0.7838	0.7727	0.7722	0.7681	0.7668	0.7285
$1s \to 3s$	0.8825	0.8799	0.8800	0.8786	0.8789	0.8350
$1s \to 4s$	0.9130	0.9120	0.9121	0.9115	0.9117	0.8672
$1s \to 5s$	0.9263	0.9258	0.9259	0.9256	0.9257	0.8811
$1s \to 6s$	0.9333	0.9331	0.9331	0.9329	0.9330	0.8883
$1s \to 2p$	0.8144	0.8062	0.8058	0.8140	0.8139	0.7706
$1s \to 3p$	0.8906	0.8885	0.8885	0.8899	0.8899	0.8456
$1s \to 4p$	0.9163	0.9154	0.9154	0.9159	0.9159	0.8714
$1s \to 5p$	0.9280	0.9275	0.9276	0.9278	0.9278	0.8832
$1s \to 6p$	0.9343	0.9340	0.9340	0.9342	0.9342	0.8895
Mean abs. dev.[c]	0.0462	0.0435	0.0434	0.0438	0.0437	
Mean percentage error	5.50%	5.15%	5.14%	5.19%	5.18%	

[a]Using the lowest 34 unoccupied orbitals of s and p symmetry, respectively.
[b]Nonrelativistic variational calculation [38].
[c]Mean value of the absolute deviations from the exact values.

Table 8: Singlet-triplet separations in neutral helium calculated from the X-only potential and the SIC-potential and by using various approximate XC kernels. Calculated from Eq. (23), using the lowest 34 unoccupied orbitals of s and p symmetry. All values are in mHartrees.

	x-only		SIC		
State	$f_{\rm xc}^{\rm ALDA}$	$f_{\rm x}^{\rm TDOEP}$	$f_{\rm xc}^{\rm ALDA}$	$f_{\rm xc}^{\rm TDOEP-SIC}$	exact[b]
$2S$	32.5	44.9	34.9	37.1	29.3
$3S$	9.3	10.7	9.5	9.3	7.4
$4S$	4.0	4.2	4.0	3.7	2.9
$5S$	2.1	2.1	2.1	1.9	1.4
$6S$	1.2	1.2	1.2	1.1	0.8
$2P$	7.1	16.2	8.6	7.8	9.3
$3P$	2.7	4.9	3.0	3.1	2.9
$4P$	1.2	2.1	1.3	1.4	1.3
$5P$	0.6	1.1	0.6	0.7	0.6
$6P$	0.3	0.6	0.4	0.4	0.4
dev.[c]	1.46	4.26	1.98	2.26	
rel. dev.	35%	49%	37%	31%	

[a]Including correlation contributions in the form of Vosko, Wilk and Nusair [49].
[b]Taken from Ref. [46]
[c]Mean absolute deviation from the exact values

between the exact 1s eigenvalue ($\epsilon_{1s}^{\rm exact} = -0.90372$ a.u.) and the more strongly bound 1s eigenvalue of the X-only potential ($\epsilon_{1s}^{\rm X-only} = -0.91796$ a.u.). Similarly, the Kohn-Sham eigenvalue differences calculated in OEP-SIC are shifted by up to 44.5 mH, which again is equal to the difference between the 1s eigenvalues of the exact Kohn-Sham potential and the KS potential in OEP-SIC. In OEP-SIC, the correlation potential is attractive at all points in space. Hence, including SIC-correlation contributions into the OEP worsens the occupied orbital eigenvalue. To summarize, the inclusion of correlation contributions to the ground state potential mostly affects only the occupied state; the virtual states are almost exact, i.e., they are almost independent of the choice of the correlation potential. The He Kohn-Sham orbitals exhibit a Rydberg-like behavior already for relatively low quantum numbers n [41]: already the lower virtual states are mostly determined by the large-r behavior of the Kohn-Sham potential, which is governed by the exchange contribution.

As a consequence, the corrections to the Kohn-Sham orbital energy differences, calculated on the approximate orbitals, are very close to the corrections calculated from the exact Kohn-Sham orbitals. This is most apparent from the singlet-triplet splittings given in tables 3 and 8: the splittings depend more strongly on the choice of the XC kernel than on the choice of the potential. However, for the excitation energies, the differences among the various approximations of the exchange correlation kernel are *smaller* than the differences in the Kohn-Sham excitation energies coming from different potentials. This reflects the fact that the resulting orbitals are rather insensitive to different approximations of the potential. Hence, the corrections themselves, calculated with approximate XC *kernels* will not cancel the shortcomings of an approximate exchange *potential*. Tables 4 - 7 show that the corrections go in the right direction only for the singlet states, which are always lower

than the corresponding Kohn-Sham orbital energy differences. In other approximations, like the LDA and in the popular GGAs for instance, this will be even more severe: There the highest occupied orbital eigenvalue is in error by about a factor of two, due to spurious self-interaction. There may be error cancellations for the lower Kohn-Sham eigenvalue differences, but in general one should not expect to get a reliable (Kohn-Sham) spectrum in LDA and GGAs, because the respective potentials have the wrong behavior for large r. In addition, this causes the number of (unoccupied) bound KS states to be *finite*.

In total, the inaccuracies introduced by *approximate* ground state Kohn-Sham potentials are substantial, but mostly reside in the occupied eigenvalue for He. It is very unlikely that these defects will be cured by better approximations of $f_{\rm xc}$ alone, since the terms containing $f_{\rm xc}$ only give corrections to the underlying Kohn-Sham eigenvalue spectrum. Hence, the quantitative calculation of excitation energies heavily depends on the accuracy of the ground-state potential employed.

5 Results for the Beryllium Atom

5.1 Exact Kohn-Sham potential

The beryllium atom serves as a further standard example for first principles treatments: besides numerous quantum chemical studies (e.g. [52, 53]), a highly accurate ground-state exchange-correlation potential, obtained from quantum Monte-Carlo methods [54], is available for this system. With this potential, we calculated accurate Kohn-Sham orbitals and orbital energies of the beryllium atom. In each symmetry class (s, p, and d), up to 38 virtual states were calculated on a radial grid similar to the one used in section 4.

In tables 9 and 10 we report the excitation energies for the 11 lowest excitations of singlet and triplet symmetry. As in helium, the orbital energies of the accurate potential lie always in between the experimental singlet and triplet energies. However, the experimentally measured singlet-triplet separations in beryllium are much larger than in the helium atom (cf. the last columns given in tables 3 and 11). Accordingly, to achieve agreement with the experimental data, appreciable shifts of the Kohn-Sham eigenvalue differences are needed.

For the singlet excitation spectrum, given in table 9, the TDDFT corrections yield significantly improved excitation energies compared to spectrum of the bare Kohn-Sham eigenvalue differences, with average errors reduced by a factor of about 3 regardless of which kernel is used. The most distinct improvement towards experiment is achieved for the singlet 2P excitation, where the Kohn-Sham eigenvalue difference is off by 32% (61 mHartree) from the experimental value.

For the remaining singlet excitations, the TDOEP-SIC kernel yields the best improvement upon the bare Kohn-Sham spectrum. From figure 2, where the errors for each singlet excitation energy are plotted, we see two competing effects: the errors increase with progressing angular momentum (with the error of the 3d-states being largest), but decrease with progressing principal quantum number n. Note that ALDA has the largest errors for the d-states, presumably due to its inability to account for orbital nodes.

For the triplet spectrum given in table 10, the transition to the 2p state is clearly problematic, presumably because of its small magnitude. In particular, the TDOEP X-only calculation greatly underestimates the downshift away from the KS eigenvalue difference.

Table 9: Singlet excitation energies for the Be atom, calculated from the exact XC potential by using approximate XC kernels (in atomic units)

		ALDA (xc)		TDOEP (x-only)		TDOEP (SIC)		
$k \to j$	ω_{jk}	SPA	full[a]	SPA	full[a]	SPA	full[a]	Expt. [b]
$2s \to 2p$	0.1327	0.2078	0.1889	0.2040	0.1873	0.2013	0.1855	0.1939
$2s \to 3s$	0.2444	0.2526	0.2515	0.2574	0.2553	0.2566	0.2547	0.2491
$2s \to 3p$	0.2694	0.2690	0.2714	0.2748	0.2758	0.2739	0.2750	0.2742
$2s \to 3d$	0.2833	0.2783	0.2779	0.2851	0.2851	0.2843	0.2842	0.2936
$2s \to 4s$	0.2959	0.2983	0.2984	0.2994	0.2995	0.2993	0.2994	0.2973
$2s \to 4p$	0.3046	0.3045	0.3049	0.3063	0.3067	0.3061	0.3065	0.3063
$2s \to 4d$	0.3098	0.3084	0.3084	0.3106	0.3106	0.3104	0.3103	0.3134
$2s \to 5s$	0.3153	0.3163	0.3164	0.3168	0.3170	0.3167	0.3169	0.3159
$2s \to 5p$	0.3193	0.3192	0.3194	0.3201	0.3203	0.3200	0.3202	0.3195
$2s \to 6s$	0.3247	0.3252	0.3253	0.3254	0.3256	0.3254	0.3256	0.325
$2s \to 6p$	0.3269	0.3268	0.3269	0.3273	0.3274	0.3272	0.3273	0.327
Mean abs. dev.[c]	0.0081	0.0043	0.0031	0.0031	0.0028	0.0029	0.0029	
Mean rel. dev.	3.75%	1.69%	1.15%	1.27%	1.09%	1.13%	1.15%	
abs. dev.[d]	0.0028	0.0033	0.0029	0.0025	0.0025	0.0024	0.0024	
rel. dev.[d]	0.97%	1.14%	1.01%	0.87%	0.86%	0.86%	0.83%	

[a]Using the lowest 38 unoccupied orbitals of s, p and d symmetry, respectively.
[b]Experimental values from Ref. [55].
[c]Mean value of the absolute deviations from experiment, (all states tabulated)
[d]Same as [c], but excluding the $2s \to 2p$ transition.

Because of this effect, we also report average errors with this transition excluded. All Kohn-Sham orbital excitations experience a downshift in the ALDA and TDOEP X-only calculation. In ALDA, this leads to an overall improvement of the spectrum by a more than a factor of 2. The downshift in TDOEP X-only results is too strong, and this behavior is partly corrected in the TDOEP-SIC. However, due to overcorrections for the higher excitation energies, the average reduction in error over the Kohn-Sham excitation spectrum is only a factor of 1.2.

The errors for the triplet excitation energies are plotted in figure 3. Clearly, the errors of both the Kohn-Sham eigenvalue spectrum and the corresponding corrections decrease again with progressing quantum number. Together with the errors plotted in figure 2 this signals that the Rydberg-like transitions to states with high principal quantum number n are already close to the eigenvalue differences of the accurate Kohn-Sham potential.

The singlet-triplet separations from equation (23) are given in table 11 for the three different approximate XC kernels. Like in helium, the singlet-triplet splittings are overestimated by about a factor of two for the S and P transitions if the (diagonal) TDOEP x-only kernel is used. The splittings of the D levels, however, appear too *small* by about a factor of two. By the inclusion of correlation contributions to the kernels, the splittings of the S and P levels are consistently (and usually correctly) reduced. However, for the D states, this correction is always too large, and leads to a reversal of the singlet and triplet energies.[3]

[3]This effect can also be observed in the Helium atom. The exact values of the singlet-triplet splittings of the D states in helium however, are by two orders of magnitude smaller than in beryllium.

Table 10: Triplet excitation energies for the Be atom, calculated from the exact XC potential by using approximate XC kernels (in atomic units)

		ALDA (xc)		TDOEP (X-only)		TDOEP (SIC)		
$k \to j$	ω_{jk}	SPA	full[a]	SPA	full[a]	SPA	full[a]	Expt. [b]
$2s \to 2p$	0.1327	0.0982	0.0902	0.0679	0.0000	0.0916	0.0795	0.1002
$2s \to 3s$	0.2444	0.2390	0.2387	0.2349	0.2338	0.2431	0.2430	0.2373
$2s \to 3p$	0.2694	0.2651	0.2651	0.2647	0.2652	0.2700	0.2705	0.2679
$2s \to 3d$	0.2833	0.2807	0.2805	0.2814	0.2813	0.2867	0.2865	0.2827
$2s \to 4s$	0.2959	0.2943	0.2943	0.2932	0.2934	0.2953	0.2953	0.2939
$2s \to 4p$	0.3046	0.3031	0.3032	0.3031	0.3034	0.3048	0.3049	0.3005
$2s \to 4d$	0.3098	0.3087	0.3087	0.3098	0.3089	0.3106	0.3107	0.3096
$2s \to 5s$	0.3153	0.3146	0.3146	0.3142	0.3143	0.3150	0.3150	0.3144
$2s \to 5p$	0.3193	0.3186	0.3187	0.3187	0.3188	0.3194	0.3194	0.3193
$2s \to 6s$	0.3247	0.3243	0.3243	0.3241	0.3242	0.3245	0.3245	0.3242
$2s \to 6p$	0.3269	0.3265	0.3265	0.3265	0.3266	0.3269	0.3269	0.3268
Mean abs. dev.[c]	0.0045	0.0012	0.0020	0.0040	0.0102	0.0026	0.0037	
Mean rel. dev.	3.53%	0.56%	1.28%	3.31%	9.51%	1.44%	2.55%	
abs. dev.[d]	0.0017	0.0012	0.0012	0.0012	0.0013	0.0020	0.0020	
rel. dev.[d]	0.63%	0.42%	0.41%	0.42%	0.46%	0.72%	0.74%	

[a]Using the lowest 38 unoccupied orbitals of s, p and d symmetry, respectively.
[b]Experimental values from Ref. [55].
[c]Mean value of the absolute deviations from experiment
[d]Same as [c], but excluding the $2s \to 2p$ transition.

From the singlet-triplet splitting in Eq. (40) which, in the SPA, hold for any system since the diagonal terms of $f_{\mathrm{xc}\sigma\sigma'}$ cancel, this behavior can be traced back to the overestimation of correlation contributions in LDA (in small systems). Self-interaction corrections are not expected to cure this shortcoming, for the reason that to leading order the self-interaction correction terms cancel in the expressions for the splittings, similar to the way shown in section 4. Accordingly, the separations in TDOEP-SIC and ALDA are of similar quality, which can be seen from columns one and three in table 11. The TDOEP X-only results on the other hand, although too small, show the correct ordering of singlet and triplet levels.

With increasing excitation energy, the difference between the results in SPA and the full solution is reduced, as was already observed in the case of helium. The drastic change of the triplet $2P$ state in TDOEP X-only seems to be an artifact of the specific approximation to the exchange-correlation kernel, since the results in the SPA and the full calculation for this particular excitation energy only differ by 10% if the ALDA is used for $f_{\mathrm{xc}\sigma\sigma'}$.

5.2 Approximate Kohn-Sham potentials

The results from using different approximate exchange-correlation *potentials* for the Be atom to calculate the Kohn-Sham eigenvalues and orbitals are given in tables 12 to 15.

The errors towards the experimental excitation energies are compiled in figures 2 and 3 for the singlet and triplet series. Looking first at the spectra of the bare Kohn-Sham eigenvalues (represented in figures 2 and 3 by the points connected with thick lines), we notice that the

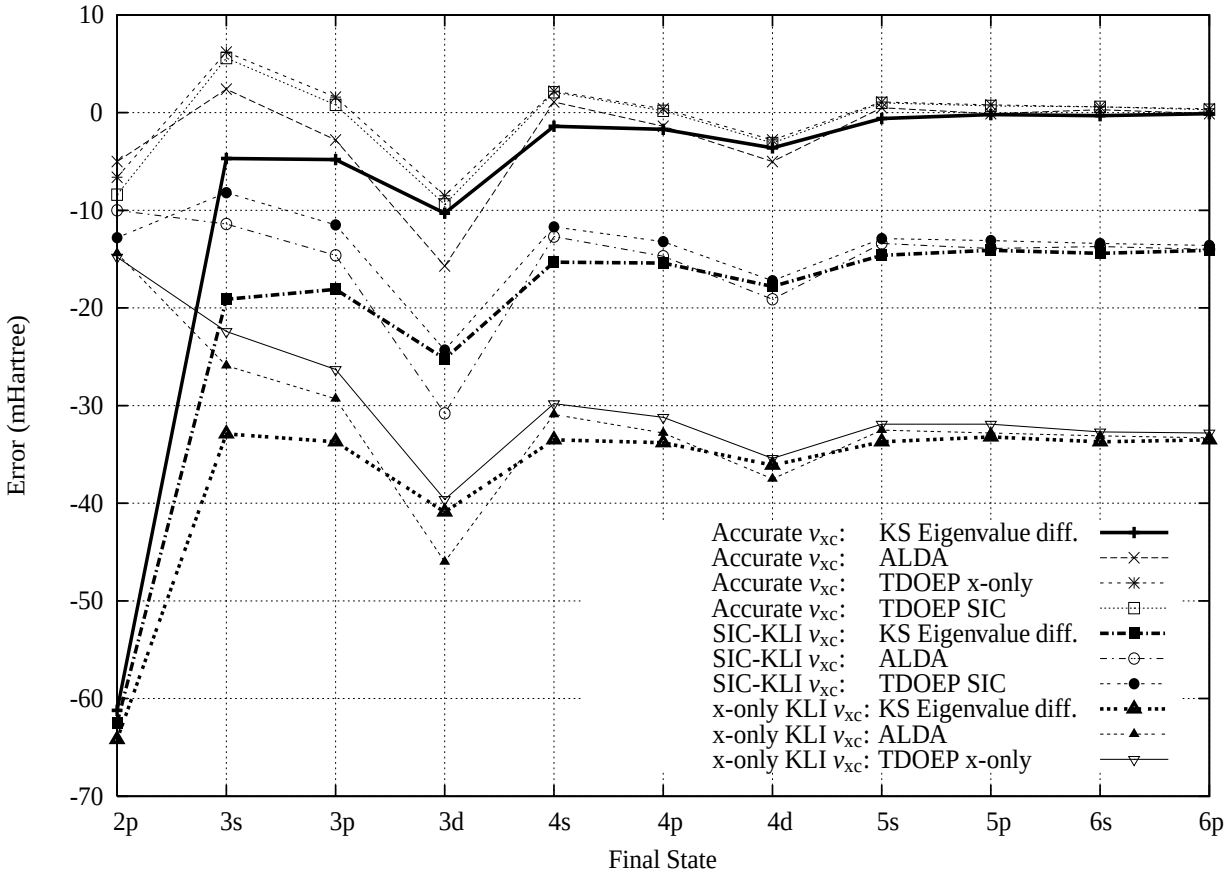

Figure 2: Errors of singlet excitation energies from the ground state of Be, calculated from the accurate, the OEP-SIC and X-only KLI exchange correlation potential and with different approximations for the exchange-correlation kernel (see text). The errors are given in mHartrees. To guide the eye, the errors of the discrete excitation energies were connected with lines.

"HOMO-LUMO" gap is almost independent of the approximation of $v_{\rm xc}$ employed. This is in sharp contrast with the He atom case. The correlation contributions cancel for the lowest excitation energy, and we must classify this as a non-Rydberg state. For the higher states, the situation is different: Starting from the excitation to the 3s level, the series of single-particle energy differences appear almost *uniformly shifted* with respect to the series of the exact potential, preserving the typical pattern of their deviation from the experimentally measured spectrum. The shifts amount to -14 mH for the OEP-SIC potential, and -34 mH for the X-only KLI potential. As in helium, these shifts are equal to the differences in the eigenvalues of the highest occupied Kohn-Sham orbital: For the accurate potential ($\epsilon_{2s}^{\rm accurate} = -0.3426$ a.u. [56]), the highest occupied orbitals are more strongly bound than in OEP-SIC ($\epsilon_{2s}^{\rm OEP-SIC} = -0.3285$ a.u.) and in X-only KLI ($\epsilon_{2s}^{\rm X-onlyKLI} = -0.3089$ a.u.). Thus, among the virtual states, only the 2p orbital is appreciably influenced by the details of the ground state potential. For the higher lying states, the long-range behavior of the Kohn-Sham potential dominates. Its $-1/r$ behavior is correctly reproduced both in X-only KLI as well as in OEP-SIC. For larger systems, more low-lying excitations can be accurately

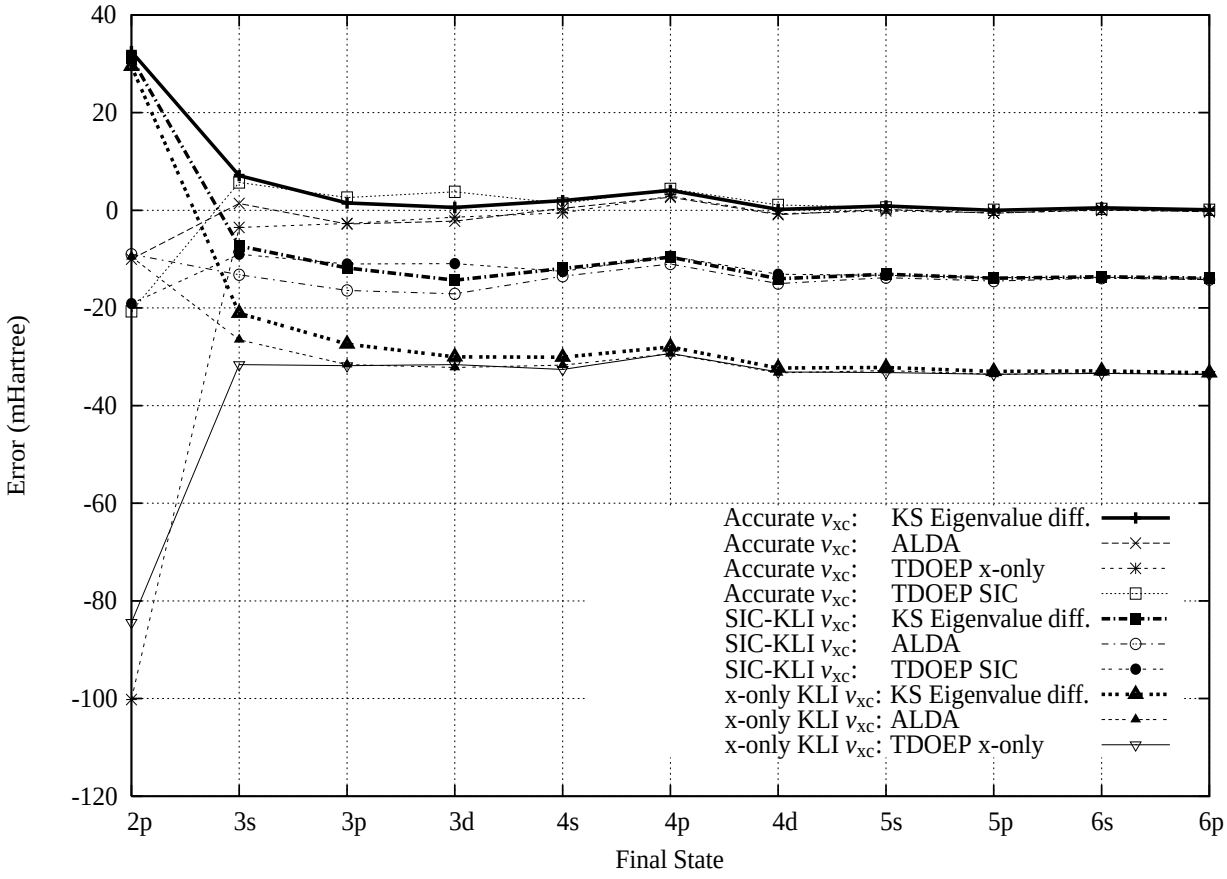

Figure 3: Errors of triplet excitation energies from the ground state of Be, calculated from the accurate, OEP-SIC and X-only KLI exchange correlation potential and with different approximations for the exchange-correlation kernel (see text). The errors are given in mHartrees. To guide the eye, the errors of the discrete excitation energies were connected with lines.

approximated, but eventually, for any finite system, the Rydberg excitations will show errors due to errors in the ionization potential. Casida et al.[23] have studied which excitations can be well-approximated with present functional approximations to the potential.

Regarding the corrections for the singlet excitation energies calculated from Eq. (23), the first excited state (2p) experiences the largest correction, irrespective of the exchange-correlation potential employed. Moreover, the results using different approximate exchange-correlation kernels agree within 10 mH. For the remaining singlet excitation energies, the calculated corrections using the approximate Kohn Sham orbitals are almost identical to the corrections which are obtained from using the accurate Kohn-Sham orbitals. Hence, in figure 2 the errors for the excitations to 3s through 6p show the same pattern of deviations, only shifted by the error in the respective eigenvalue of the 2s orbital. On average, the resulting singlet excitation energies are closest to experiment, if the approximate exchange-correlation potential $v_{\rm xc}$ is combined with the corresponding approximation of the exchange-correlation kernel $f_{{\rm xc}\,\sigma\sigma'}$.

From tables 13 and 15 as well as from figure 3, the behavior of the triplet spectra is

Table 11: Singlet-triplet separations in beryllium calculated from the exact XC potential by using various approximate XC kernels. Calculated from Eq. (23), using the lowest 38 unoccupied orbitals of s, p and d symmetry. All values are in mHartrees.

	ALDA	TDOEP		
State	XC[a]	X-only	SIC	Expt.[b]
$2P$	98.7	187.3	106.0	93.8
$3S$	12.8	21.5	11.8	11.8
$3P$	6.2	10.5	4.6	6.4
$3D$	-2.6	3.8	-2.3	10.8
$4S$	4.1	6.1	4.1	3.4
$4P$	1.7	3.4	1.6	5.8
$4D$	-0.2	1.7	-0.3	3.8
$5S$	1.8	2.7	1.9	2.4
$5P$	0.7	1.5	0.8	0.2
$6S$	1.0	1.4	1.0	0.6
$6P$	0.3	0.8	0.4	–
dev.[c]	3.0	12.4	3.8	
rel. dev.	68%	128%	75%	

[a]Including correlation contributions in the form of Vosko, Wilk and Nusair [49].
[b]Taken from Ref. [55]
[c]Mean absolute deviation from experiment, excluding the $6P$ state.

similar, but less unequivocal for the triplet 2p state. For this particular state, the corrections spread on the order of 100mH, prevalently due to the significant overcorrection of the X-only TDOEP kernels. However, the resulting triplet 2p excitation energy almost exclusively depends on the approximation to the exchange correlation kernel rather than on the exchange-correlation potential employed. On the average, apart from the higher excitations in OEP-SIC (c.f. table 14), the best triplet spectra are obtained if the ALDA is used for the exchange-correlation kernel, but this appears to be a fortuitous cancellation of errors. The approximate Kohn-Sham excitation energies, except for the 2p state, are already incorrectly lower than the experimental triplet levels. Any further lowering, although correct for the eigenvalue-differences of the exact Kohn-Sham potential, actually worsens the triplet spectra which are calculated on the basis of an approximate exchange-correlation potential. Since the shifts are reduced by correlation contributions in the kernels, the over-corrections become less severe for the ALDA and TDOEP-SIC kernels. Another apparent error cancellation is that when calculating the lowest excitation energy ($2s \rightarrow 2p$) from approximate exchange-correlation potentials, the SPA-results are always closer to experiment than the full results. This might be related to the fact that for TDOEP X-only, SPA yields the exact first-order shift in energy levels in Görling-Levy perturbation theory[57], while the "full" calculation does not[48]. In cases where there are large differences between SPA and full results, the SPA might be more reliable for these reasons.

The fact that the corrections to the Kohn-Sham eigenvalue differences only weakly depend on the approximation of the exchange-correlation potential $v_{\rm xc}$, is also reflected in table 16, where the singlet-triplet separations in Be, calculated using the X-only KLI

Table 12: Singlet excitation energies for the Be atom, calculated from the X-only KLI potential by using approximate XC kernels (in atomic units)

		ALDA (xc)		TDOEP (X-only)		
$k \to j$	ω_{jk}	SPA	full[a]	SPA	full[a]	Expt. [b]
$2s \to 2p$	0.1297	0.1990	0.1795	0.1958	0.1791	0.1939
$2s \to 3s$	0.2162	0.2245	0.2232	0.2288	0.2267	0.2491
$2s \to 3p$	0.2405	0.2415	0.2449	0.2465	0.2479	0.2742
$2s \to 3d$	0.2527	0.2480	0.2476	0.2541	0.2540	0.2936
$2s \to 4s$	0.2638	0.2663	0.2664	0.2674	0.2675	0.2973
$2s \to 4p$	0.2725	0.2727	0.2735	0.2745	0.2751	0.3063
$2s \to 4d$	0.2773	0.2758	0.2759	0.2780	0.2780	0.3134
$2s \to 5s$	0.2822	0.2833	0.2834	0.2838	0.2840	0.3159
$2s \to 5p$	0.2863	0.2864	0.2867	0.2872	0.2876	0.3195
$2s \to 6s$	0.2913	0.2918	0.2919	0.2921	0.2923	0.325
$2s \to 6p$	0.2935	0.2936	0.2937	0.2940	0.2942	0.327
Mean abs. dev.[c]	0.0372	0.0311	0.0317	0.0288	0.0299	
Mean rel. dev.[d]	13.5%	10.4%	10.7%	9.5%	10.1%	
abs. dev.[d]	0.0345	0.0337	0.0334	0.0315	0.0314	
rel. dev.[d]	11.49%	11.18%	11.07%	10.39%	10.38%	

[a]Using the lowest 38 unoccupied orbitals of s, p and d symmetry, respectively.
[b]Experimental values from Ref. [55].
[c]Mean value of the absolute deviations from experiment
[d]Same as [c], but excluding the $2s \to 2p$ transition.

and OEP-SIC potentials are given. The numerical values are close to the results for the accurate Be exchange correlation potential in table 11. Again, the obtained splittings are more sensitive to the approximation of $f_{\mathrm{xc}\sigma\sigma'}$ than to the approximation of the potential v_{xc}.

6 Summary and Conclusion

In this work we aimed at an assessment of the influence of the three different types of approximations (i.e. (i) the XC potential v_{xc}, (ii) the XC kernel f_{xc} and (iii) truncation of the space of virtual excitations) inherent in the calculation of excitation energies from TDDFT. We calculated the discrete optical spectra of helium and beryllium, two of the spectroscopically best known elements, using the exact exchange-correlation potential, the KLI-X-only potential and the the KLI-SIC potential for v_{xc} (all three potentials are falling off like $-1/r$ as $r \to \infty$). These were combined with three approximations for the XC kernel: The adiabatic LDA (ALDA), the TDOEP X-only kernel and the TDOEP-SIC kernel. The results are given both in the single-pole approximation (SPA) and for a "full" calculation, where as many virtual states as possible (typically about 30 to 40) entered the calculation. The analysis of these combinations reveals the following trends: First of all, the choice of v_{xc} on the calculated spectrum has the largest effect on the calculated spectra. The inaccuracies introduced by *approximate* ground state Kohn-Sham potentials (even those including exact exchange) can be quite substantial. This is especially true for the higher excited states,

Table 13: Triplet excitation energies for the Be atom, calculated from the X-only KLI potential by using approximate XC kernels (in atomic units)

		ALDA (xc)		TDOEP (X-only)		
$k \to j$	ω_{jk}	SPA	full[a]	SPA	full[a]	Expt. [b]
$2s \to 2p$	0.1297	0.0980	0.0907	0.0692	0.0158	0.1002
$2s \to 3s$	0.2162	0.2112	0.2108	0.2069	0.2057	0.2373
$2s \to 3p$	0.2405	0.2362	0.2363	0.2353	0.2361	0.2679
$2s \to 3d$	0.2527	0.2506	0.2505	0.2512	0.2511	0.2827
$2s \to 4s$	0.2638	0.2622	0.2622	0.2611	0.2613	0.2939
$2s \to 4p$	0.2725	0.2710	0.2711	0.2709	0.2712	0.3005
$2s \to 4d$	0.2773	0.2763	0.2763	0.2765	0.2765	0.3096
$2s \to 5s$	0.2822	0.2815	0.2816	0.2811	0.2812	0.3144
$2s \to 5p$	0.2863	0.2856	0.2857	0.2856	0.2857	0.3193
$2s \to 6s$	0.2913	0.2909	0.2909	0.2907	0.2908	0.3242
$2s \to 6p$	0.2935	0.2931	0.2932	0.2931	0.2932	0.3268
Mean abs. dev.[c]	0.0300	0.0291	0.0298	0.0323	0.0371	
Mean rel. dev.	11.8%	9.9%	10.6%	12.8%	17.6%	
abs. dev.[d]	0.0300	0.0318	0.0318	0.0324	0.0324	
rel. dev.[d]	10.1%	10.7%	10.7%	11.0%	11.0%	

[a]Using the lowest 38 unoccupied orbitals of s, p and d symmetry, respectively.
[b]Experimental values from Ref. [55].
[c]Mean value of the absolute deviations from experiment
[d]Same as [c], but excluding the $2s \to 2p$ transition.

which appear almost uniformly shifted from the true excitation energies. We observe that this shift is closely related to the absolute value of the highest occupied eigenvalue, which, in exact DFT, is equal to the first ionization potential of the system at hand.

For the lower excitation energies, an error cancellation occurs, making these excitations less sensitive to the choice of the exchange-correlation potential. This error cancellation however, ceases to work the more the excited states behave like Rydberg states. For Helium, this is already the case for the first excited state. Hence, in improving the calculation of excitation energies from TDDFT requires an improved exchange-correlation potential in the first place. The most important requirement for such a potential would be that its highest occupied eigenvalue reproduces the experimental ionization potential as closely as possible. Empirically, one could introduce a "scissors-operator" similar to the one introduced by Levine and Allan [58], which shifts the Rydberg states by a constant being equal to the difference between the highest occupied eigenvalue and the negative of the experimental ionization potential. But such a procedure would not produce a *first-principles* calculation. In our opinion however, the construction of approximate exchange-correlation potentials based on orbital functionals would be the method of choice for the future.

The effect of the choice of the exchange-correlation *kernel* on the calculated spectra, in turn, is much less pronounced. However, its relative importance increases whenever the "first-order" effects, originating from $v_{\rm xc}$ cancel. This is the case for the values of the singlet-triplet splittings and the lower excitation energies of Be. For these "second-order effects", the correlation contributions contained in $f_{\rm xc}$ are important. We observe that the

Table 14: Singlet excitation energies for the Be atom, calculated from the SIC-KLI potential by using approximate XC kernels (in atomic units)

		ALDA (xc)		TDOEP (SIC)		
$k \to j$	ω_{jk}	SPA	full[a]	SPA	full[a]	Expt. [b]
$2s \to 2p$	0.1314	0.2030	0.1839	0.1968	0.1811	0.1939
$2s \to 3s$	0.2300	0.2390	0.2377	0.2429	0.2409	0.2491
$2s \to 3p$	0.2561	0.2566	0.2596	0.2614	0.2627	0.2742
$2s \to 3d$	0.2684	0.2632	0.2628	0.2694	0.2693	0.2936
$2s \to 4s$	0.2820	0.2844	0.2846	0.2855	0.2856	0.2973
$2s \to 4p$	0.2909	0.2910	0.2916	0.2926	0.2931	0.3063
$2s \to 4d$	0.2956	0.2943	0.2943	0.2961	0.2962	0.3134
$2s \to 5s$	0.3013	0.3023	0.3025	0.3028	0.3030	0.3159
$2s \to 5p$	0.3054	0.3054	0.3056	0.3062	0.3064	0.3195
$2s \to 6s$	0.3106	0.3112	0.3113	0.3114	0.3116	0.325
$2s \to 6p$	0.3129	0.3129	0.3130	0.3133	0.3134	0.327
Mean abs. dev.[c]	0.0210	0.0155	0.0153	0.0130	0.0138	
Mean rel. dev.[d]	8.07%	5.29%	5.25%	4.32%	4.78%	
abs. dev.[d]	0.0168	0.0161	0.0158	0.0140	0.0139	
rel. dev.[d]	5.65%	5.35%	5.26%	4.60%	4.60%	

[a]Using the lowest 38 unoccupied orbitals of s, p and d symmetry, respectively.
[b]Experimental values from Ref. [55].
[c]Mean value of the absolute deviations from experiment
[d]Same as [c], but excluding the $2s \to 2p$ transition.

ALDA for the XC kernels already leads to quite reasonable results which are only marginally improved by using the more complicated TDOEP-SIC kernel. Besides the missing frequency dependence, correlation contributions are hard to model on top of an exact exchange treatment and one might speculate that the ALDA takes advantage from a fortuitous error cancellation between exchange and correlation effects. Again, we expect only orbital functionals to manage a marked improvement over the ALDA, which, up to now, can has been the workhorse of TDDFT.

Finally, the inevitable truncation of the space of virtual excitations is appreciable only for the lowest lying states. In most cases, the results of the single-pole approximation (SPA), which, in the nondegenrate case, merely requires a pair of "initial" and "final" KS states are close to the results obtained from using more configurations.

We thank C. Umrigar for providing us with the data of the exact exchange-correlation potentials for helium and beryllium. This work was supported in part by the Deutsche Forschungsgemeinschaft and by NATO. K.B. acknowledges support of the Petroleum Research Fund and of NSF grant CHE-9875091.

References

[1] P. Hohenberg and W. Kohn, Phys. Rev. **136**, B864 (1964).

[2] O. Gunnarsson and B.I. Lundqvist, Phys. Rev. B **13**, 4274 (1976).

Table 15: Triplet excitation energies for the Be atom, calculated from the SIC-KLI potential by using approximate XC kernels (in atomic units)

		ALDA (xc)		TDOEP (SIC)		
$k \to j$	ω_{jk}	SPA	full[a]	SPA	full[a]	Expt. [b]
$2s \to 2p$	0.1314	0.0987	0.0912	0.0925	0.0811	0.1002
$2s \to 3s$	0.2300	0.2245	0.2241	0.2284	0.2283	0.2373
$2s \to 3p$	0.2561	0.2515	0.2515	0.2563	0.2569	0.2679
$2s \to 3d$	0.2684	0.2658	0.2656	0.2720	0.2718	0.2827
$2s \to 4s$	0.2820	0.2804	0.2804	0.2814	0.2814	0.2939
$2s \to 4p$	0.2909	0.2894	0.2895	0.2910	0.2911	0.3005
$2s \to 4d$	0.2956	0.2946	0.2946	0.2965	0.2965	0.3096
$2s \to 5s$	0.3013	0.3006	0.3006	0.3010	0.3011	0.3144
$2s \to 5p$	0.3054	0.3047	0.3048	0.3055	0.3055	0.3193
$2s \to 6s$	0.3106	0.3103	0.3103	0.3105	0.3105	0.3242
$2s \to 6p$	0.3129	0.3125	0.3126	0.3129	0.3129	0.3268
Mean abs. dev.[c]	0.0141	0.0131	0.0138	0.0117	0.0127	
Mean rel. dev.	6.58%	4.52%	5.22%	4.39%	5.41%	
abs. dev.[d]	0.0123	0.0142	0.0143	0.0121	0.0121	
rel. dev.[d]	4.13%	4.83%	4.84%	4.06%	4.04%	

[a]Using the lowest 38 unoccupied orbitals of s, p and d symmetry, respectively.
[b]Experimental values from Ref. [55].
[c]Mean value of the absolute deviations from experiment
[d]Same as [c], but excluding the $2s \to 2p$ transition.

[3] T. Ziegler, A. Rauk, and E.J. Baerends, Theoret. Chim. Acta **43**, 261 (1977).

[4] U. von Barth, Phys. Rev. A **20**, 1693 (1979).

[5] A. Theophilou, J. Phys. C **12**, 5419 (1979).

[6] W. Kohn, Phys. Rev. A **34**, 5419 (1986).

[7] E.K.U. Gross, L.N. Oliveira, and W. Kohn, Phys. Rev. A **37**, 2805 (1988).

[8] E.K.U. Gross, L.N. Oliveira, and W. Kohn, Phys. Rev. A **37**, 2809 (1988).

[9] L.N. Oliveira, E.K.U. Gross, and W. Kohn, Phys. Rev. A **37**, 2821 (1988).

[10] A. Nagy, Phys. Rev. A **42**, 4388 (1990).

[11] A. Nagy, Int. J. Quantum Chem. Symp. **29**, 297 (1995).

[12] M. Levy, Phys. Rev. A **52**, R4313 (1995).

[13] A. Görling, Phys. Rev. A **54**, 3912 (1996).

[14] M. Petersilka, U.J. Gossmann, and E.K.U Gross, Phys. Rev. Lett. **76**, 1212 (1996).

[15] E. Runge and E.K.U. Gross, Phys. Rev. Lett. **52**, 997 (1984).

Table 16: Singlet-triplet separations in beryllium calculated from the X-only potential and the SIC-potential and by using various approximate XC kernels. Calculated from Equation (23), using the lowest 38 unoccupied orbitals of s, p and d symmetry, respectively. All values are in mHartrees.

	X-only		SIC		
State	$f_{\rm xc}^{\rm ALDA}$	$f_{\rm x}^{\rm TDOEP}$	$f_{\rm xc}^{\rm ALDA}$	$f_{\rm xc}^{\rm TDOEP-SIC}$	Expt.[b]
$2P$	88.9	163.3	92.7	100.1	93.8
$3S$	12.4	21.0	13.6	12.5	11.8
$3P$	8.6	11.8	8.0	5.9	6.4
$3D$	-2.9	2.9	-2.8	-2.5	10.8
$4S$	4.1	6.2	4.2	4.2	3.4
$4P$	2.4	3.9	2.1	2.0	5.8
$4D$	-0.4	1.4	-0.2	-0.4	3.8
$5S$	1.9	2.7	1.8	1.9	2.4
$5P$	1.0	1.8	0.8	0.9	0.2
$6S$	1.0	1.5	1.0	0.4	0.6
$6P$	0.5	1.0	0.4	0.5	–
dev.[c]		3.1	10.2	2.8	3.1
rel. dev.		85%	145%	75%	75%

[a]Including correlation contributions in the form of Vosko, Wilk and Nusair [49].
[b]Taken from Ref. [55]
[c]Mean absolute deviation from the exact values

[16] M. Petersilka and E.K.U. Gross, Int. J. Quantum Chem. **60**, 181 (1996).

[17] R. Bauernschmitt and R. Ahlrichs, Chem. Phys. Lett. **256**, 454 (1996).

[18] *Time-dependent density functional response theory of molecular systems: Theory, computational methods, and functionals*, M.E. Casida, in *Recent developments and applications in density functional theory*, ed. J.M. Seminario (Elsevier, Amsterdam, 1996).

[19] R. Bauernschmitt, M. Hauser, O. Treutler, and R. Ahlrichs, Chem. Phys. Lett. **264**, 573 (1997).

[20] T. Grabo, Ph.D. thesis, Universität Würzburg, 1997.

[21] S.J.A. van Gisbergen, F. Kootstra, P.R.T. Schipper, O.V. Gritsenko, J.G. Snijders, and E.J. Baerends, Phys. Rev. A **57**, 2556 (1998).

[22] M.E. Casida, K.C. Casida, and D.R. Salahub, Int. J. Quant. Chem. **70**, 933 (1998).

[23] M.E. Casida, C. Jamorski, K.C. Casida, and D.R. Salahub, J. Chem. Phys. **108**, 4439 (1998).

[24] T. Grabo, M. Petersilka, and E.K.U. Gross, Phys. Rev. A (1999), in press.

[25] D. Sundholm, Chem. Phys. Lett., **302**, 480 (1999).

[26] J.P. Perdew and A. Zunger, Phys. Rev. B **23**, 5048 (1981).

[27] J.B. Krieger, Y. Li, and G.J. Iafrate, Phys. Lett. A **146**, 256 (1990).

[28] J.B. Krieger, Y. Li, and G.J. Iafrate, Phys. Rev. A **45**, 101 (1992).

[29] J.B. Krieger, Y. Li, and G.J. Iafrate, Phys. Rev. A **46**, 5453 (1992).

[30] J.B. Krieger, Y. Li, and G.J. Iafrate, in *Density Functional Theory*, Vol. 337 of *NATO ASI Series B*, edited by E.K.U. Gross and R.M. Dreizler (Plenum Press, New York, 1995), p. 191.

[31] J. Chen, J.B. Krieger, Y. Li, and G.J. Iafrate, Phys. Rev. A **54**, 3939 (1996).

[32] A.L. Fetter and J.D. Walecka, *Quantum Theory of Many-Particle Systems* (McGraw-Hill, New York, 1971).

[33] K.L. Liu and S.H. Vosko, Can. J. Phys. **67**, 1015 (1989).

[34] E.K.U. Gross, J.F. Dobson, and M. Petersilka, in *Density Functional Theory II*, Vol. 181 of *Topics in Current Chemistry*, edited by R.F. Nalewajski (Springer, Berlin, 1996), p. 81.

[35] E.K.U. Gross and W. Kohn, Adv. Quant. Chem. **21**, 255 (1990).

[36] A. Görling and M. Levy, Phys. Rev. B **47**, 13105 (1993).

[37] R.T. Sharp and G.K. Horton, Phys. Rev. **90**, 317 (1953).

[38] J.D. Talman and W.F. Shadwick, Phys. Rev. A **14**, 36 (1976).

[39] C.A. Ullrich, U.J. Gossmann, and E.K.U. Gross, Phys. Rev. Lett. **74**, 872 (1995).

[40] R. van Leeuwen, Phys. Rev. Lett. **80**, 1280 (1998).

[41] M. Petersilka, U. Gossmann, and E.K.U. Gross, in *Electronic Density Functional Theory: Recent Progress and New Directions*, edited by G. Vignale J.F. Dobson and M.P. Das (Plenum, New York, 1998), p. 177.

[42] *Orbital functionals in density functional theory: the optimized effective potential method*, T. Grabo, T. Kreibich, S. Kurth, and E.K.U. Gross, in *Strong Coulomb correlations in electronic structure: Beyond the local density approximation*, ed. V.I. Anisimov (Gordon and Breach, Tokyo, 1998).

[43] *Density Functional Theory of Time-Dependent Phenomena*, E.K.U. Gross, J.F. Dobson, and M. Petersilka, Topics in Current Chemisty, **181**, 81 (1996).

[44] L.V. Chernysheva, N.A. Cherepkov, and V. Radojević, Comput. Phys. Commun. **11**, 57 (1976).

[45] C.J. Umrigar and X. Gonze, Phys. Rev. A **50**, 3827 (1994).

[46] A. Kono and S. Hattori, Phys. Rev. A **29**, 2981 (1984).

[47] *Relationship of Kohn-Sham eigenvalues to excitation energies*, A. Savin, C.J. Umrigar, X. Gonze, Chem. Phys. Lett. **288**, 391 (1998).

[48] *A hybrid functional for the exchange-correlation kernel in time-dependent density functional theory*, K. Burke, M. Petersilka, and E.K.U. Gross, in *Recent advances in density functional methods, vol. III*, ed. P. Fantucci and A. Bencini (World Scientific Press, 2000).

[49] S.H. Vosko, L. Wilk, and M. Nusair, Can. J. Phys. **58**, 1200 (1980).

[50] E. Engel, J.A. Chevary, L.D. Macdonald, and S.H. Vosko, Z. Phys. D **23**, 7 (1992).

[51] C.O. Almbladh and U. von Barth, Phys. Rev. B **31**, 3231 (1985).

[52] L. Zülicke, *Quantenchemie* (Hüthig, Heidelberg, 1985), Vol. 2.

[53] R.L. Graham, D.L. Yeager, J. Olsen, P. Jørgensen, R. Harrison, S. Zarrabian, and R. Bartlett, J. Chem. Phys. **85**, 6544 (1986).

[54] C.J. Umrigar and X. Gonze, a preliminary version was published in *High Performance Computing and its Application to the Physical Sciences*, proceedings of the Mardi Gras '93 Conference, edited by D. A. Browne et al., (World Scientific, Singapore, 1993) (unpublished).

[55] S. Bashkin and J.A. Stoner, Jr., *Atomic Energy Levels and Grotrian Diagrams I* (North-Holland, Amsterdam, 1975).

[56] C. Filippi, X. Gonze, and C.J. Umrigar, in *Recent Developments and Applications of Density Functional Theory*, edited by J.M. Seminario (Elsevier, Amsterdam, 1996).

[57] X. Gonze and M. Scheffler, Phys. Rev. Lett. **82**, 4416 (1999).

[58] Z.H. Levine and D.C. Allan, Phys. Rev. Lett. **63**, 1719 (1989).